Effect of Offset Mismatch in Time-Interleaved ADC Circuits on OFDM-BER Performance

Vo-Trung-Dung Huynh, Nele Noels, *Member, IEEE,* and Heidi Steendam, *Senior Member, IEEE*

***Abstract*—This paper analyses the effect of the offset mismatch in time-interleaved analog-to-digital converter (TI-ADC) circuits on bit error rate (BER) performance of a receiver for pulse amplitude modulated (PAM) or quadrature amplitude modulated (QAM) signals in orthogonal frequency division multiplexed (OFDM) systems. Exact BER expressions, as well as simplified BER expressions that hold for high signal-to-noise ratios (SNRs) and large offset mismatch values only, are derived. From the obtained exact BER expressions, a condition is established on the offset mismatch level, under which the BER performance shows an error floor at high SNRs. Numerical results further show that if we keep the offset mismatch level below 25% of the threshold above which the offset mismatch causes an error floor, there is essentially no BER performance degradation compared to the offset-mismatch free case. Our analysis further evinces that the tolerable level of the offset mismatch is proportional to the square-root of the number of sub-ADCs, indicating that as opposed to what might be expected, the offset mismatch level that can be tolerated actually increases with the number of sub-ADCs.**

***Index Terms*—Time-interleaved ADC, offset mismatch, bit error rate, PAM, QAM, OFDM.**

I. Introduction

MANY wired and wireless standards employ orthogonal frequency division multiplexing (OFDM) because of its high spectral efficiency and tolerance against channel dispersion. Recently, OFDM was proposed to be used in multi-Gigabit fiber-optic communication systems (see [1] and the references therein). In such high-speed fiber-optic OFDM systems, the analog-to-digital converters (ADCs) placed prior to the baseband digital signal processor core are required to operate at extremely high sampling rates. Further, OFDM is considered for software defined radio [2], where analog-to-digital conversion is performed before downconversion of the bandpass signal, to facilitate reconfigurability of the system. This also requires the ADC to operate at a very high sampling rate. Because the development of such high-sampling-rate ADCs collides with the physical constraints of the current technology [3], ADCs employing a time-interleaved (TI) architecture are often considered as an attractive low-cost alternative. In a TI-ADC [4], several slower sampling-rate sub-ADCs are placed in parallel. The lth sub-ADC will sample the signal at time instants $t_k^{(l)} = CK_l + kLT_s$, where $k = 0, 1, 2, ...$, $l = 0, 1, ..., L-1$, and L is the number of sub-ADCs. The clock references $CK_l = CK_0 + lT_s$ are equidistantly shifted in time with as spacing the desired sampling time T_s. Therefore, the overall sampling rate $\frac{1}{T_s}$ is L times higher than the sampling rate $\frac{1}{LT_s}$ of each individual sub-ADC. Unfortunately, mismatches between the parallel sub-ADCs, due to fabrication process variations, form a major obstacle towards the practical use of such TI-ADC architectures. One of the most challenging problems is offset mismatch, which refers to differences in the DC levels that are employed by the various sub-ADCs [5]. The effect of the offset mismatch on the system performance has recently been studied in [6]-[11] for single-carrier systems and in [12]-[16] for multi-carrier systems. However, to the best of our knowledge, an analysis of a non-negligible offset mismatch on the bit error rate (BER) performance of OFDM systems employing a TI-ADC has not been studied yet.

In this paper, we first analytically derive exact BER expressions for PAM- and QAM-OFDM systems, assuming binary reflected Gray code (BRGC) bit mapping [19]. Previous investigations reported a BER floor at high signal-to-noise ratios (SNRs) in the case of severe offset mismatch [16]. The BER expressions obtained here allow to determine a condition on the offset mismatch values, that will result in an error floor. Our expressions further reveal that in the case of a very severe offset mismatch, the induced BER floor is essentially independent of the modulation order, the modulation type and the channel. Finally, a rule-of-thumb is derived for determining the maximum level of offset mismatch that can be tolerated to guarantee a negligible BER performance degradation with respect to the mismatch-free case. This tolerable offset mismatch level can serve as a guideline for circuits-and-systems design engineers to compensate the offset mismatch through hardware calibration or digital signal processing.

The remainder of the paper is organized as follows. Table I illustrates the notations used in the following sections. Section II presents the signal model at the output of a TI-ADC with fixed offset mismatches, and at the output of the subsequent discrete Fourier transform (DFT) unit in an OFDM system. In Section III, we theoretically derive the exact BER expression for an OFDM system with rectangular QAM signaling. The BER expressions include the special cases of square QAM and PAM. The condition for the error floor occurrence as well as simplified expressions for the error floor caused by severe offset mismatch are derived in Section IV. In Section V, we validate the accuracy of the derived expressions by comparing their numerical evaluation with the result of a brute-force Monte Carlo simulation, and we analyse the effect of the offset mismatch on the BER performance. We also derive a rule-of-thumb for a tolerable offset mismatch level causing

V-T-D. Huynh, N. Noels and H. Steendam are with the DIGCOM research group, TELIN Department, Ghent University, 9000 Ghent, Belgium (email: {votrungdung.huynh, nele.noels, heidi.steendam}@ugent.be).

This research has been funded by the Interuniversity Attraction Poles Programme initiated by the Belgian Science Policy Office. The authors acknowledge the financial support from the Flemish fund for Scientific Research (FWO).

TABLE I
NOTATION EXPLANATION

Notation	Meaning
I_d	the collection of indices of data sub-carriers
$\beta \in \{I, Q\}$	the in-phase (I) or quadrature (Q) dimension
m_β	information bits in the β-dimension
N	FFT size
N_{CP}	the cyclic prefix length
L	the number of sub-ADCs
E_s	the transmitted symbol energy
N_0	the variance of Gaussian noise samples
do_l	the offset voltage of the lth sub-ADC
$do_l^{(x\%)}$	the offset voltage of the lth sub-ADC at $x\%$ mismatch
σ_{do}^2	the variance of the random offset values do_l
K	the set of indices of data sub-carriers affected by offset mismatch
d_β	the half minimum Euclidean distance in the β-dimension

negligible BER performance degradation. Section VI presents the conclusions of the study.

II. SYSTEM MODEL

The block diagram of the considered OFDM system is shown Fig. 1. To simplify the notations, we consider the transmission of a single OFDM block. Let us define I_d as the collection of indices of all sub-carriers that are used for data transmission[1], where $I_d \subset \left\{-\frac{N}{2}, -\frac{N}{2}+1, ..., \frac{N}{2}-1\right\}$ and N is a power of 2. A sequence of $|I_d|_c \cdot (m_I + m_Q)$ bits is divided into $|I_d|_c$ blocks of $(m_I + m_Q)$ bits, where $|I_d|_c$ is the cardinality of I_d. Each sub-block of $(m_I + m_Q)$ information bits is mapped onto the in-phase and quadrature components of a unit-energy $M_I \times M_Q$ rectangular QAM symbol ($M_I = 2^{m_I}$, $M_Q = 2^{m_Q}$) according to a 2-dimensional m_I-by-m_Q bit BRGC [19]. The symbols $X[n]$, $n \notin I_d$, are set to zero for the non-modulated carriers, i.e., $X[n] = 0$ for $n \notin I_d$, in order to form the vector $\mathbf{X} = \left(X\left[-\frac{N}{2}\right], X\left[-\frac{N}{2}+1\right], ..., X\left[\frac{N}{2}-1\right]\right)^T$, which is applied to an inverse discrete Fourier transform (IDFT) of size N. The resulting time-domain samples are extended with a cyclic prefix (CP) of length N_{CP} samples to avoid inter-carrier and inter-symbol interference (ICI and ISI), caused by a dispersive channel. The time-domain samples $s[k]$ are given by:

$$s[k] = \sqrt{\frac{N}{N+N_{CP}}} \cdot \frac{1}{\sqrt{N}} \sum_{a=-\frac{N}{2}}^{\frac{N}{2}-1} X[a] e^{j2\pi \frac{ak}{N}}, \quad -\frac{N}{2} - N_{CP} \leq k \leq \frac{N}{2} - 1, \tag{1}$$

where the pre-factor $\sqrt{\frac{N}{N+N_{CP}}}$ originates from the loss of energy efficiency due to the insertion of the CP. Before transmission over the channel, the time-domain samples pass through a digital-to-analog converter (DAC) and a transmit filter.

At the receiver, after passing through the receive filter, the received waveform is sampled at Nyquist rate by a TI-ADC. The TI-ADC is assumed to have a sufficiently high resolution so that the quantization noise can be neglected in this analysis [20]-[21]. Furthermore, since the offset voltages in a TI-ADC are only slowly time varying [15], we model them as constants over the duration of an OFDM symbol period[2]. Using the model of a TI-ADC with offset mismatch introduced in [17], the output of the TI-ADC can be written as:

$$\begin{aligned} r[k] &= \sqrt{E_s} \cdot s[k] \otimes h[k] \\ &+ \sqrt{E_s} \cdot \sum_{l=0}^{L-1} \sum_{q=-\infty}^{\infty} do_l \cdot \delta[k - qL - l] \\ &+ w[k], \\ &k = -\frac{N}{2} - N_{CP}, -\frac{N}{2} - N_{CP} + 1..., \frac{N}{2} - 1, \end{aligned} \tag{2}$$

where $r[k]$ is the kth received sample, $h[k]$ is the sampled impulse response of the channel, $\otimes$ denotes the discrete convolution operation, $\delta[.]$ denotes the discrete dirac function, $s[k]$ is defined by (1), E_s is the transmitted symbol energy, do_l is the offset voltage of the lth sub-ADC, expressed relative to E_s, and $w[k]$ are statistically independent Gaussian noise samples with zero mean and variance $\frac{N_0}{2}$ per I/Q dimension. When all sub-ADCs have identical offset voltages, the second term in (2) reduces to a sample-independent constant. As this DC component can easily be compensated by the receiver, we do not consider this to be an offset mismatch. Only when the offset voltages do_l are not equal, we say the TI-ADC suffers from offset mismatch. In the following, we assume that the transmit and receive filter are perfectly matched. Further, we assume that the receiver has perfect knowledge about the channel, and knows the start of the OFDM blocks, i.e., "perfect timing synchronization". The receiver removes the CP and converts the remaining N samples to the frequency domain. Before data detection, the receiver multiplies the DFT outputs with $\frac{1}{H[n]}\sqrt{\frac{N+N_{CP}}{N}}$, where $H[n]$ is the discrete frequency response of the channel, to compensate for the channel coefficient and the loss in energy, i.e., "perfect equalization". This yields

$$\begin{aligned} R_{DFT}[n] &= \frac{1}{H[n]}\sqrt{\frac{N+N_{CP}}{N}} \cdot \frac{1}{\sqrt{N}} \sum_{k=-\frac{N}{2}}^{\frac{N}{2}-1} r[k] e^{-j2\pi \frac{kn}{N}} \\ &= \sqrt{E_s} X[n] + \sqrt{E_s} \frac{DO[n]}{\mathscr{H}[n]} + \frac{W[n]}{\mathscr{H}[n]}, \\ &n = -\frac{N}{2}, -\frac{N}{2}+1, ..., \frac{N}{2}-1, \end{aligned} \tag{3}$$

where $X[n]$ are the transmitted symbols, $\mathscr{H}[n] \triangleq \sqrt{\frac{N}{N+N_{CP}}} H[n]$, $W[n]$ are statistically independent Gaussian random variables with zero mean and variance $\frac{N_0}{2}$, and $DO[n]$ is a function of the offset voltages do_l from the

[1]In many OFDM systems, not all sub-carriers are modulated for data transmission. For example, a few sub-carriers near the edges (i.e., the guard band) are not modulated to obtain a reasonable transition band at the bandwidth boundaries as well as to simplify the transmit and receive filter designs [18].

[2]In practice, the offset values can vary over time due to multiple causes, e.g., supply voltage variations, temperature and ageing effects. If the power supply noise is at a high frequency, this might cause the non-negligible variation of the offset during an OFDM symbol. However, this scenario would almost certainly destroy the operation of the entire signal processing chain and hence should be resolved by adequate power supply decoupling. Therefore, in a proper designed system, the power supply noise effect should not be a limitation in reality. Also temperature and ageing effects can cause offset variations. However, these effects occur on a time scale that is several orders of magnitude slower than the OFDM symbol rate, and hence the assumption of the fixed offset voltages over an OFDM symbol is still valid.

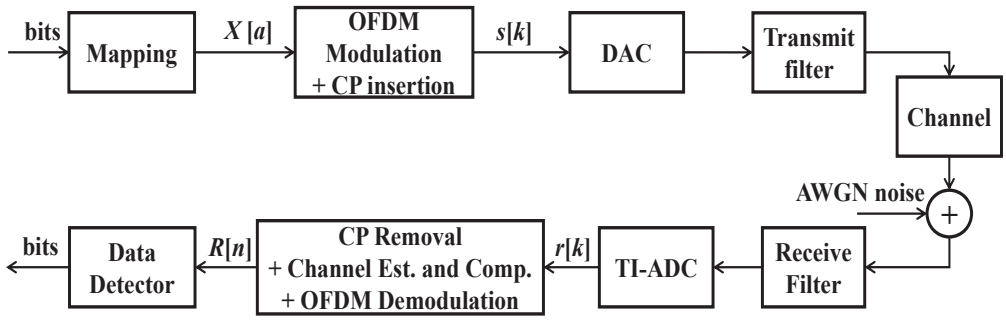

Fig. 1. Block diagram of an OFDM system with a TI-ADC at the receiver.

L sub-ADCs:

$$DO[n] = \frac{\sqrt{N}}{L} \sum_{i=-\frac{L}{2}}^{\frac{L}{2}-1} \sum_{l=0}^{L-1} do_l e^{-j2\pi \frac{i}{L} l} \delta\left[n - i\frac{N}{L}\right]. \quad (4)$$

To simplify the expressions, we assumed in (4) that the number L of sub-ADCs is a power of 2. Further, in (4), it is assumed that the ratio $\frac{N}{L}$ between the IDFT/DFT size and the number of sub-ADCs is an integer value. However, an extension to non-integer ratios $\frac{N}{L}$ is straightforward[3]. Finally, the quantities $R_{\mathrm{DFT}}[n]$ from (3) at the DFT output are used to perform bit sequence detection by determining the constellation point at minimum Euclidean distance from $R_{\mathrm{DFT}}[n]$ and applying the inverse mapping rule.

Let us take a closer look at the contribution of $DO[n]$ from (4) to the $R_{\mathrm{DFT}}[n]$ from (3). Inspecting (4) reveals that only sub-carriers with indices $i\frac{N}{L}$ ($i \in \mathbb{Z}$) are affected by a data-independent contribution from the offset mismatch. Further, we notice that $DO[0]$ and $DO\left[-\frac{N}{2}\right]$ are real-valued, whereas all other contributions $DO[n]$ are complex-valued with $DO[-n] = (DO[n])^*$, where $(x)^*$ denotes the complex conjugate of a complex number x. The offset values do_l can be modelled as independent and identically distributed (i.i.d) zero-mean random variables with variance σ_{do}^2 [5]. The DFT output $DO[n]$ is therefore a zero-mean random variable with autocorrelation function: $E\left[DO[n](DO[n'])^*\right] = \frac{N}{L}\sigma_{do}^2 \delta[n-n'],\ n = i\frac{N}{L}, i \in \mathbb{Z}$, i.e., the contributions on the different sub-carriers are uncorrelated. Furthermore, for the cases where $DO[n]$ is complex-valued, $DO[n]$ is circularly invariant, implying its real and imaginary parts have the same variance $\frac{N}{2L}\sigma_{do}^2$. Later in this paper, we will show that the BER performance of the OFDM system is determined by the largest absolute value of the real and imaginary parts of $\frac{DO[n]}{\mathscr{H}[n]}$. Hence, we are interested in the probability that $\left|\left(\frac{DO[n]}{\mathscr{H}[n]}\right)^{(\beta)}\right|$ exceeds a given value, where $|x|$ denotes the absolute value of x, $\beta \in \{I, Q\}$ refers to the in-phase and quadrature dimensions of the signal, and $(x)^{(\beta)}$ is defined as:

$$(x)^{(\beta)} = \begin{cases} \Re\{x\} & \text{, if } \beta = I \\ \Im\{x\} & \text{, if } \beta = Q \end{cases}, \quad (5)$$

where $\Re\{x\}$ and $\Im\{x\}$ are the real and imaginary part of x, respectively. When L is sufficiently large, the distribution of $DO[n]$ approaches (according to the central limit theorem) a Gaussian distribution. As a result, the probability that $\left|\left(\frac{DO[n]}{\mathscr{H}[n]}\right)^{(\beta)}\right|$ exceeds the value θ is given by:

$$\Pr\left[\left|\left(\frac{DO[n]}{\mathscr{H}[n]}\right)^{(\beta)}\right| > \theta\right] = erfc\left(\frac{\theta \cdot |\mathscr{H}[n]|}{\sqrt{2}\sigma_\beta[n]}\right), \quad (6)$$

where

$$\sigma_\beta^2[n] = \begin{cases} \frac{N\sigma_{do}^2}{2L} & \text{, if } n = i\frac{N}{L}, i \in \mathbb{Z}\backslash\left\{0, -\frac{L}{2}\right\}, \beta \in \{I, Q\} \\ \frac{N\sigma_{do}^2}{L} & \text{, if } n \in \left\{0, -\frac{N}{2}\right\}, \beta = I \\ 0 & \text{, if } n \in \left\{0, -\frac{N}{2}\right\}, \beta = Q \end{cases}, \quad (7)$$

and $erfc(.)$ is the complementary error function [22].

III. BER Derivation

To compute the BER, we only have to take into account the data-bearing sub-carriers, i.e., with indices $n \in I_d$. Let us define the set K that collects the indices of all modulated sub-carriers affected by the offset mismatch, i.e., $K = \left\{n \in I_d | n = i\frac{N}{L}, i \in \mathbb{Z}\right\}$. Hence, the BER for a given channel $\mathbf{h}$, i.e., $BER_{|\mathbf{h}}$, can be decomposed as:

$$\begin{aligned} BER_{|\mathbf{h}} = & \frac{1}{|I_d|_c} \sum_{n \in I_d \backslash K} BER_{|\mathbf{h}, no\,off, n} \\ & + \frac{1}{|I_d|_c} \sum_{n \in K} BER_{|\mathbf{h}, off, n} \end{aligned}, \quad (8)$$

where $BER_{|\mathbf{h}, no\,off, n}$ is the BER for a given $\mathbf{h}$, which stems from the sub-carriers that are not disturbed by the offset mismatch, i.e., with indices $n \in I_d \backslash K$, and $BER_{|\mathbf{h}, off, n}$ is the BER for a given $\mathbf{h}$, originating from the offset-mismatch affected sub-carriers, i.e., with indices $n \in K$. The terms in the first sum depend on the sub-carrier index through the dependency of the channel frequency response $\mathscr{H}[n]$ only, whereas for the terms in the second sum, the sub-carrier dependency is due to the dependency of both $\mathscr{H}[n]$ and $DO[n]$ on the sub-carrier index.

In [23], a closed-form expression for the BER of a generalized amplitude-modulated transmission was derived, assuming an AWGN channel and BRGC mapping for an ideal ADC (i.e., $do_l = 0$). Extending the result from [23] to a dispersive channel characterized by the coefficients $\{\mathscr{H}[n]\}$, the terms $BER_{|\mathbf{h}, no\,off, n}$ in the first sum of (8) can be written as (see

[3]In this case, the dirac function in (4) is replaced by the sinc function, which is defined as: $\mathrm{sinc}(x) = \frac{\sin(\pi x)}{\pi x}$.

Appendix A):

$$BER_{|\mathbf{h},no\,off,n} = \frac{1}{(m_I+m_Q)} \sum_{\beta,u,v} \frac{R_v^{(u,\beta)}}{M_\beta} erfc\left((2v+1)\,d_\beta \left|\mathscr{H}[n]\right| \sqrt{\frac{E_s}{N_o}}\right), \tag{9}$$

where m_I and m_Q are the number of bits transmitted on the symbol's in-phase and quadrature components, $M_\beta = 2^{m_\beta}$, $u \in \{1, ..., m_\beta\}$, and $v \in \{0, 1, ..., (1-2^{-u})\,M_\beta - 1\}$. In (9), the quantity $R_v^{(u,\beta)}$ is a short-hand notation for the following function of β, u and v:

$$R_v^{(u,\beta)} = (-1)^{\left\lfloor \frac{v\cdot 2^{u-1}}{M_\beta} \right\rfloor} \cdot \left(2^{u-1} - \left\lfloor \frac{v\cdot 2^{u-1}}{M_\beta} + \frac{1}{2} \right\rfloor\right), \tag{10}$$

where $\lfloor x \rfloor$ denotes the largest integer smaller than x, and d_β is the half minimum Euclidean distance between the constellation points in the $\beta-$dimension[4] [24]:

$$d_\beta = \sqrt{\frac{3z_\beta(\zeta)}{(M_I^2-1) + \left(M_Q^2-1\right)\zeta^2}}, \tag{11}$$

where $\zeta = \frac{d_Q}{d_I}$, and $z_\beta(\zeta)$ is defined as: $z_\beta(\zeta) = 1$, if $\beta = I$ and $z_\beta(\zeta) = \zeta^2$, if $\beta = Q$.

In the remainder of this section, we further extend the closed-form expression from [23] to take into account the effect of the invariant offset mismatch, in order to find a closed-form expression for the BER of the affected sub-carriers, i.e., with indices $n \in K$. The derivation of $BER_{|\mathbf{h},off,n}$ in (8) can be found in Appendix A. In the derivation, we assume that the offset voltages are fixed. This is a reasonable assumption, as the random offset mismatch values vary very slowly with time [15]. Hence, the BER for given offset voltages reflects the error performance of a given TI-ADC realization. We obtain:

$$BER_{|\mathbf{h},\,off,n} = \frac{1}{2(m_I+m_Q)} \cdot \sum_{\alpha,\beta,u,v} \frac{R_v^{(u,\beta)}}{M_\beta} \cdot erfc\left(\left((2v+1)\,d_\beta + \alpha\cdot\left(\frac{DO[n]}{\mathscr{H}[n]}\right)^{(\beta)}\right)\left|\mathscr{H}[n]\right|\sqrt{\frac{E_s}{N_0}}\right), \tag{12}$$

where $\alpha \in \{-1, 1\}$, and $(DO[n])^{(\beta)}$ is defined in (5). Note that the BER in (12) is not only for a given TI-ADC realization, but also for a given channel realization. If for sub-carrier n the channel realization $\mathscr{H}[n]$ is small, e.g., a deep fade, the effect of the offset mismatch $\left(\frac{DO[n]}{\mathscr{H}[n]}\right)^{(\beta)}$ will be relatively larger compared to when $\mathscr{H}[n]$ is large.

Substituting (9) and (12) into (8) yields the exact closed-form BER expression for $M_I \times M_Q$-QAM signaling in the presence of offset mismatch. The corresponding result for M_s-ary square QAM signaling follows from setting M_I and M_Q equal to $\sqrt{M_s}$, and d_Q equal to d_I. Similarly, the general BER expression for M_p-ary PAM signaling can be obtained by setting M_I equal to M_p, and M_Q equal to 1. Note that in this case $\Im\left\{\frac{DO[n]}{\mathscr{H}[n]}\right\}$ has no effect on the BER performance, so the summation over β disappears in (9) and (12).

In the case of fibre-optic [25] or wired RF communication, the channel can be modelled as a (quasi) time-invariant channel over many OFDM blocks, implying (8) represents the BER of the link. However, in wireless communication, most channels exhibit time variation, where the channel can be modelled as quasi-static over one or a few OFDM blocks, and the channel taps are to be modelled as random variables. In such time-varying channels, the average BER needs to be computed by averaging (8) over the distribution of the channel:

$$BER = \int_{\mathbf{h}} BER_{|\mathbf{h}} \cdot p_{PDF}(\mathbf{h}) d\mathbf{h}, \tag{13}$$

where $p_{PDF}(\mathbf{h})$ is the probability density function (pdf) of $\mathbf{h}$.

IV. The Error Floor

In this section, we investigate the high SNR behavior of the BER expressions derived in Section III. The complementary error function (erfc-function) $erfc(x)$ in (9) and (12) is a strictly monotonically decreasing function of its argument x, with a very small slope for large absolute values of x and asymptotes $erfc(-\infty) = 2$ and $erfc(+\infty) = 0$. It follows that (9) and all terms in (12) with strictly positive arguments of the erfc-function vanish for large SNR, whereas the terms in (12) with negative arguments of the erfc-function saturate to an SNR independent value for $\frac{E_s}{N_0}$ going to infinity. It follows immediately that:

- A condition for the occurrence of a floor in the BER from (8) at high SNR is therefore:

$$\min_{n,\alpha,\beta,u,v}\left((2v+1)\,d_\beta + \alpha\cdot\left(\frac{DO[n]}{\mathscr{H}[n]}\right)^{(\beta)}\right) = \min_\beta\left\{d_\beta - \max_n\left|\left(\frac{DO[n]}{\mathscr{H}[n]}\right)^{(\beta)}\right|\right\} \le 0, \tag{14}$$

or, equivalently,

$$\min_{n,\beta}\left\{\frac{d_\beta}{\max\left|\left(\frac{DO[n]}{\mathscr{H}[n]}\right)^{(\beta)}\right|}\right\} \le 1, \tag{15}$$

where the optimization is with respect to all $n \in I_d \backslash K$, $\alpha \in \{-1, 1\}$, $\beta \in \{-I, Q\}$, $u \in \{1, ..., m_\beta\}$, $v \in \{0, 1, ..., (1-2^{-u})\,M_\beta - 1\}$, and $|x|$ denotes the absolute value of x. In other words, as long as on all affected sub-carriers, the contribution $\left|\left(\frac{DO[n]}{\mathscr{H}[n]}\right)^{(\beta)}\right|$ is smaller than the half Euclidean distance d_β between the constellation points, no error floor occurs. The condition (15) enables us to determine the maximum level of offset mismatch that can be tolerated if we want to avoid a BER floor.

- The larger the number of terms in (8) for which the argument of the error function in (12) is negative, the larger the BER floor at high SNR. The maximum value of the floor occurs in the case where the argument of the erfc-function in (12) is negative for all β, u, v, and $\alpha = -sign\left(\left(\frac{DO[n]}{\mathscr{H}[n]}\right)^{(\beta)}\right)$. In that case, $BER_{|\mathbf{h}}$ (12) will be equal to $BER_{|\mathbf{h},\,off,n} = BER_{r,\max}$, where (Appendix B):

$$BER_{r,\max} = \frac{|K|_c}{2|I_d|_c} - \frac{m_I\eta_Q + m_Q\eta_I}{2|I_d|_c\,(m_I+m_Q)}, \tag{16}$$

[4] Assuming the average energy per data symbol is normalized.

for rectangular constellation, where η_I and η_Q are defined in (35). For M_s-ary square QAM, where $M_I = M_Q = \sqrt{M_s}$, the error floor (16) reduces to $BER_{s,\max} = \frac{|K|_c}{2|I_d|_c} - \frac{\eta_I+\eta_Q}{4|I_d|_c}$, which for an AWGN channel corresponds to the result proposed in [16, eq. (25)]. Similarly, for M_p-ary PAM, where $M_I = M_p$ and $M_Q = 1$, the error floor (16) equals $BER_{p,\max} = \frac{|K|_c-\eta_Q}{2|I_d|_c}$. The difference between the error floors for PAM and QAM signaling becomes small when $|K|_c$ increases, i.e., when the number of affected sub-carriers increases, which corresponds to an increasing number L of sub-ADCs. In that case, the maximum error floor becomes essentially independent of the type of modulation and of the modulation order M_β ($\beta \in \{I, Q\}$) as well as of the channel, and only depends on the number $|I_d|_c$ of modulated sub-carriers and the number L of sub-ADCs:

$$BER_{r,\max} \approx BER_{s,\max} \approx BER_{p,\max} \approx \frac{|K|_c}{2|I_d|_c}. \quad (17)$$

V. An Analysis of Offset Mismatch Effect and the Rule-of-Thumb for Tolerable Offset Mismatch Level

In this section, we first validate the accuracy of the analytical expressions derived in this paper by comparing the theoretical results with simulations. Further, we will evaluate the simplified expressions for the error floor and investigate the level of the offset mismatch that can be tolerated to avoid an error floor at high SNRs, and to assure a negligible BER degradation with respect to the mismatch-free case. To clearly isolate the effect of the offset mismatch on the BER performance, we first restrict our attention to the case of an AWGN channel, and a zero CP length, i.e., $N_{CP} = 0$, and $\mathscr{H}[n] = H[n] = 1$. At the end of the section, we will evaluate the performance in the presence of a dispersive channel and a non-zero CP length. We assume that the offset mismatch values are uniformly distributed [13]-[15] in the interval $[-\varepsilon, \varepsilon]$, with $\varepsilon = \sqrt{3}\sigma_{do}$. In a first stage, we will evaluate the BER performance of a specified TI-ADC (i.e., we generate L offset mismatch values and keep these fixed), and in a second stage, we will also evaluate the average BER performance (i.e., we generate different sets of L offset mismatch values, where each set corresponds to a different TI-ADC realization). The simulation parameters are summarized in Table II. In this table, we give the fixed offset values that will be used in the first part of this section. The first offset $do_1^{(100\%)}$ is set to 0[5], and the other offsets $do_l^{(100\%)}$ are uniformly selected in the interval $[-1; 1]$[6] [15]. Table II also shows the values of the corresponding $DO[n]^{(100\%)}$ from (4) for $L = 8$. We will vary the offset mismatch level by scaling the fixed offset values from Table I, i.e., a $x\%$ mismatch level corresponds to offset mismatch values: $do_l^{(x\%)} = \frac{x}{100} do_l^{(100\%)}$,

[5]As stated earlier in this paper, a DC offset common to all sub-ADCs can easily be compensated at the receiver. Hence, without loss of generality, we can define the common DC offset value as the DC offset of the first sub-ADC, and define the other offset mismatch values relatively to the DC offset of the first sub-ADC, so $do_1^{(100\%)} = 0$.

[6]For example, the authors in [14] mentioned a standard deviation of the offset of the order of 10 mV for an ADC, which is not optimized for offset performance, in a 65 nm CMOS technology at a supply voltage of 0.8 V.

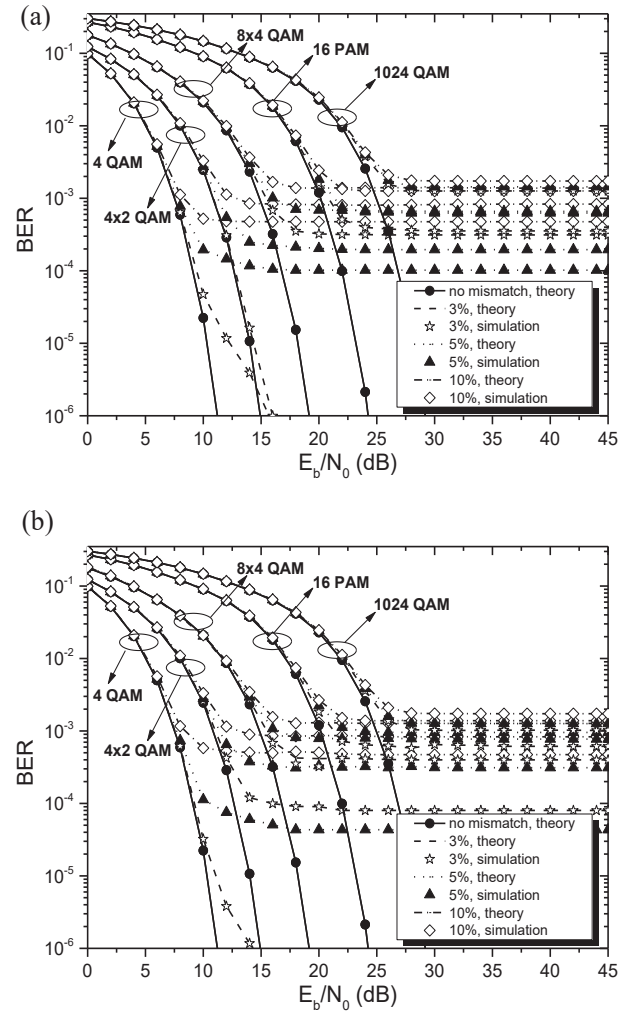

Fig. 2. BER curves of rectangular QAM ($\zeta = 2$), square QAM ($\zeta = 1$), and PAM, for 8 sub-ADCs: (a) fixed offset values, (b) random offset values.

TABLE II
Simulation Parameters

Parameters	Reference values
N	2048
$\lvert I_d\rvert_c$	1706
L	2, 4 or 8
$\zeta = \frac{d_Q}{d_I}$	1 or 2
$do_l^{(100\%)}$	$[0, 0.98, -0.59, -0.12, 0.31, -0.66, 0.41, -0.94]$
$DO[n]^{(100\%)}$ ($n \in K, L = 8$)	$[-5.034 + 15.497j, 2.772 + 7.807j, 1.526 + 4.183j, -3.451, 1.526 - 4.183j, 2.772 - 7.807j, -5.034 - 15.497j]$

and $DO[n]^{(x\%)} = \frac{x}{100} DO[n]^{(100\%)}$. Taking into account the effect of the guard band, the relationship between the SNR per symbol ($\frac{E_s}{N_0}$) and the SNR per bit ($\frac{E_b}{N_0}$), used in our simulation, is given by [26]: $\frac{E_s}{N_0} = \log_2(M_I \cdot M_Q) \cdot \frac{E_b}{N_0} \cdot \frac{|I_d|_c}{N}$.

Let us consider an AWGN channel and $N_{CP} = 0$. We first evaluate the validity of the theoretical expressions. Fig. 2 illustrates the BER performance with fixed offset values (in Table II), and the average BER performance with random offset values, for rectangular QAM, square QAM and PAM with different modulation orders when the number L of sub-

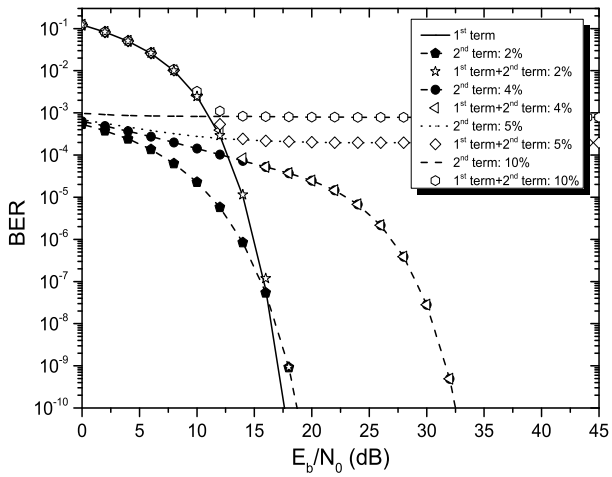

Fig. 3. BER contributions of the first and second term in (8) for 4×2-QAM ($L = 8, \zeta = 2$).

ADCs equals 8. In the figures, the BER of a system with an offset mismatch level of 3%, 5% and 10% is compared to the BER of a system without offset mismatch. It can be observed that the theoretical results are in excellent agreement with the simulation results, which demonstrates the accuracy of the proposed BER expressions. We investigated numerous other parameter settings (results not shown in this paper), and found the same excellent agreement between theory and simulations. Fig. 2 shows that an offset mismatch level that only introduces a small degradation for a small modulation order results in an error floor at higher modulation orders. This can be explained by the fact that when the modulation order increases, the half Euclidean distance d_β between the constellation points in (11) decreases. Because d_β decreases, the condition for the BER floor occurrence in (15) is easier satisfied. As a result, the error floor occurs for smaller mismatch levels.

Next, to fully understand the contribution of the affected sub-carriers on the overall BER performance, we consider Fig. 3. This figure illustrates the theoretical BER curves for 4×2-QAM, contributed by both the first and the second term in (8), for the case of 8 sub-ADCs, $\zeta = 2$ and different values for the offset mismatch level. The figure clearly shows that at high SNRs, the second term from (3) becomes the dominating contribution. This is because, for each (β, u, v), (12) will contain a term for which the argument of the erfc-function is smaller than the argument of the erfc-function for the same value of β, u, and v in (9). Further, the figure reveals that for the considered case the error floor occurs at 5% mismatch level or higher, whereas for a mismatch level of 4% or below, only a performance degradation is observed[7]. To elucidate this result, we revert to (11), (15) and Table II. Let us define a threshold γ so that the receiver will exhibit an error floor at high SNR if and only if we scale the fixed offset values $do_l^{(100\%)}$ from Table I as $\tilde{\gamma} \times do_l^{(100\%)} \left(\triangleq do_l^{(\tilde{\gamma} \times 100\%)} \right)$, with $\tilde{\gamma} \geq \gamma$. From

[7]Note that the level at which the error floor will occur, depends on the parameters of the system, e.g., the offset mismatch values, the number of sub-ADCs, the constellation, and the number of sub-carriers.

TABLE III
THE THEORETICAL MAXIMUM ERROR FLOOR VALUES

Modulation	$L = 2$	$L = 4$	$L = 8$
4 QAM	1.465×10^{-4}	7.327×10^{-4}	1.91×10^{-3}
4×2 QAM	1.953×10^{-4}	7.816×10^{-4}	1.954×10^{-3}
8×4 QAM	1.759×10^{-4}	7.62×10^{-4}	1.934×10^{-3}
16 PAM	2.93×10^{-4}	8.792×10^{-4}	2.1×10^{-3}

(15), we obtain the threshold γ:

$$\gamma = \min_{n,\beta} \left(\frac{d_\beta}{\left| \left(\frac{DO[n]^{(100\%)}}{\mathscr{H}[n]} \right)^{(\beta)} \right|} \right). \tag{18}$$

For $\mathscr{H}[n] = 1$ (AWGN channel), $L = 8$ and 4×2-QAM ($\zeta = 2$), we obtain $\gamma = 0.043$, which indicates that an error floor will occur if the offset mismatch level is larger than 4.3%. This is observed in Fig. 3: at 4% mismatch level, there is no error floor, whereas a 5% mismatch level causes an error floor. Hence, the proposed condition (15) predicts when the error floor will occur in the BER performance.

Further, we take a look at the error floor and the approximations for the error floor levels, derived in Section IV. Fig. 4 shows the effect of the number L of sub-ADCs for a large offset mismatch 100%, for the cases of 4 QAM ($\zeta = 1$), 4×2 QAM ($\zeta = 2$), 8×4 QAM ($\zeta = 2$) and 16 PAM. The values do_l of the offset mismatch correspond to the first two ($L = 2$), four ($L = 4$) and eight ($L = 8$) do_l values given in Table II, respectively. The maximum levels of the error floors obtained with (16) are shown in Table III for the different cases. Comparing Fig. 4 and Table III, it follows that the theoretical error floor from Table III corresponds well with the error floor obtained with 100% mismatch level in Fig. 4. Hence, the simple approximation (16) accurately predicts the maximum error floor. Moreover, the results clearly illustrate the increase of the maximum error floor when the number L of sub-ADCs increases. Finally, Table III demonstrates that, as predicted, the difference between the error floors for different constellation types and different modulation orders reduces when L increases. For $L = 8$, it can be observed in the table that the different maximum error floors are approximately equal for the different modulation types (QAM or PAM signaling), and modulation orders (4×2 QAM versus 8×4 QAM).

In the previous paragraph, we focussed on large offset mismatch and the threshold γ triggering the error floor. Although this level is of importance, the design engineer is more interested in tolerable levels of the offset mismatch. Therefore, we will explore the level of mismatch that causes an acceptable level of degradation. Table IV presents the threshold γ for different modulation types and different values of L. Let us now, for several offset mismatch levels $\tilde{\gamma}$, with $\tilde{\gamma} < \gamma$, consider the performance degradation compared to a system without offset mismatch at a BER[8] of 10^{-9}. Fig. 5 reveals that when reducing the mismatch level to $\tilde{\gamma} = \gamma \times 25\%$,

[8]This BER value is the standard target BER for optical communication systems [25].

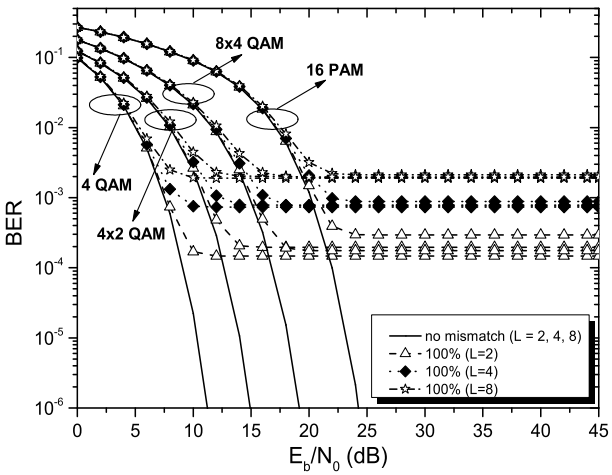

Fig. 4. BER curves for 4×2 QAM, 8×4 QAM, 4 QAM and 16 PAM signalings, and different number L of sub-ADCs.

TABLE IV
THE THRESHOLD γ

Modulation	L	γ (in %)
4 QAM ($\zeta = 1$)	8	4.562%
4×2 QAM ($\zeta = 2$)	8	4.304%
8×4 QAM ($\zeta = 2$)	4	2.51%
16 PAM	8	2.155%
1024 QAM ($\zeta = 1$)	4	0.31%
64 PAM	4	0.406%

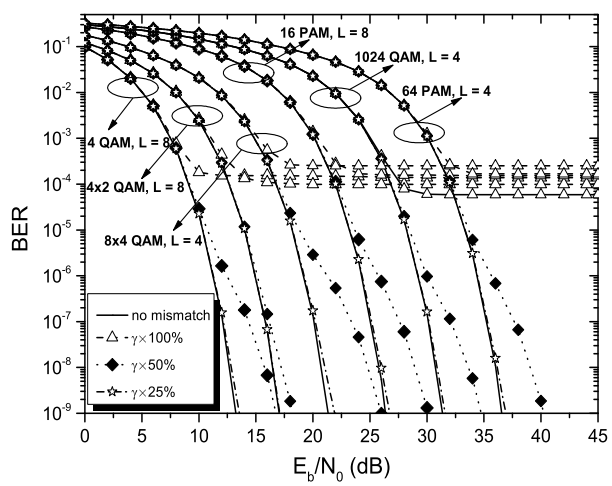

Fig. 5. BER curves for different modulation types, number of sub-ADCs and fractions of γ.

this degradation is smaller than $0.25\ dB$ for all considered cases. This observation suggests the following rule-of-thumb. If the offset mismatch level is below 25% of the threshold γ inducing the error floor, which implies that the maximum of $\left|(DO[n])^{(\beta)}\right|$ must be smaller than 25% of d_β, for both $\beta = \mathrm{I}$ and Q, no countermeasures should be taken as the degradation is at a tolerable level[9].

The above rule-of-thumb is based on the fixed values for do_l from Table II. However, in reality, the offset values are random variables. Therefore, we now investigate if the above rule-of-thumb to avoid a performance degradation is generally applicable. In this rule-of-thumb, we stated that the maximum of $\left|(DO[n])^{(\beta)}\right|$ must be smaller than 25% of d_β. However, as $(DO[n])^{(\beta)}$ is a random variable, this maximum cannot be determined straightforwardly. Moreover, when L is sufficiently large, we found in section II that $(DO[n])^{(\beta)}$ can be modelled as a Gaussian random variable, which (in theory) can reach infinitely large values. Therefore, we adapt our rule-of-thumb by imposing that in only 1% of the cases, $(DO[n])^{(\beta)}$ may be larger than 25% of d_β. Taking into account (6), for a time-invariant channel, this implies $\Pr\left[\left|\left(\frac{DO[n]}{\mathscr{H}[n]}\right)^{(\beta)}\right| > 0.25 d_\beta\right] = 0.01$ from which follows

$$\min_{n,\beta}\left(\frac{0.25 d_\beta\,|\mathscr{H}[n]|}{\sqrt{2}\sigma_\beta[n]}\right) \geq erfc^{-1}(0.01)\,, \qquad (19)$$

where $\mathscr{H}[n] = 1$ (AWGN channel), $erfc^{-1}(.)$ is the inverse erfc-function, and $\sigma_\beta[n]$ is defined in (7). Let us first consider the variance $\sigma_I^2[n]$ of the in-phase components. The variance $\sigma_I^2[0]$ of the DC component is twice the variance $\sigma_I^2\left[i\frac{N}{L}\right]$ $(i \neq 0)$ on the other sub-carriers, so the minimum over n for $\beta = I$ corresponds to the DC sub-carrier with $\sigma_I^2[0] = \frac{N\sigma_{do}^2}{L}$ (see (7)). Next, we look at the variance $\sigma_Q^2[n]$ of the quadrature components. The DC sub-carrier does not have a quadrature component, i.e., $(DO[0])^{(Q)} = 0$. For all other sub-carriers, the variance $\sigma_Q^2\left[i\frac{N}{L}\right]$ $(i \neq 0)$ is the same, i.e., $\sigma_Q^2\left[i\frac{N}{L}\right] = \frac{N\sigma_{do}^2}{2L}$ (see (7)). Expression (19) therefore reduces to $\min\left(\frac{0.25 d_I}{\sqrt{\frac{2N}{L}}\sigma_{do}}, \frac{0.25 d_Q}{\sqrt{\frac{N}{L}}\sigma_{do}}\right) \geq erfc^{-1}(0.01)$ for $L > 2$ and $\frac{0.25 d_I}{\sqrt{N}\sigma_{do}} \geq erfc^{-1}(0.01)$ for $L = 2$, as for $L = 2$ only the DC sub-carrier and the sub-carrier with index $-\frac{N}{2}$ are affected, and the sub-carrier with index $-\frac{N}{2}$ lies in the guard band. Reformulated as a condition on the standard derivation σ_{do} of the offset values, we obtain $\sigma_{do} \leq \min\left(\frac{0.25 d_I}{\sqrt{\frac{2N}{L}}erfc^{-1}(0.01)}, \frac{0.25 d_Q}{\sqrt{\frac{N}{L}}erfc^{-1}(0.01)}\right)$ if $L > 2$ and $\sigma_{do} \leq \frac{0.25 d_I}{\sqrt{N}erfc^{-1}(0.01)}$ if $L = 2$. Assuming that the offset values are uniformly distributed in $[-\varepsilon, \varepsilon]$ yielding $\sigma_{do} = \frac{\varepsilon}{\sqrt{3}}$, this provides a corresponding threshold ε_{min} on ε. Table V shows the resulting threshold ε_{min} for different modulation types and orders, for different values of L, and Fig. 6 shows the BER, averaged over the offset values, for a selection of the cases given in Table V. As can be observed from the figure, when the mismatch level equals the proposed ε_{min}, the degradation is imperceptible, whereas a degradation is visible when the mismatch level is increased to $1.75 \times \varepsilon_{min}$. Hence, the proposed rule-of-thumb indeed results in a tolerable level of the offset values. Further, we observe from Table V and the equations that the tolerable level ε_{min} of the offset values increases when L increases, i.e., ε_{min} is proportional to $\sqrt{L}$. This counterintuitive result can be explained as follows. When L increases, the number of affected sub-carriers increases, but on each of these affected sub-carriers, the disturbance $DO[n]$ will be smaller, as its variance $\sigma_\beta^2[n]$ (7) reduces. Hence, on each of the affected sub-carriers, the probability

[9]This rule-of-thumb was successfully checked for other modulation types and orders, and for other numbers of sub-ADCs, than shown in the figure.

$BER_{off,n}$ reduces. When the level of the mismatch is below the threshold inducing the error floor, the overall BER will therefore reduce with increasing L. This is illustrated in Fig. 7. This is in contrast to the case where the offset mismatch level exceeds the error floor threshold. In that case, the overall BER increases with L, as was also observed in the simplified expressions for the error floor in Section IV. The reason for this is that for large offset mismatch levels, the erfc-function in $BER_{off,n}$ saturates so that $BER_{off,n}$ becomes independent of n.

Now, we will extend the BER performance evaluation and the rule-of-thumb (19) for an AWGN channel to a time-varying dispersive channel, e.g., a multi-path Rayleigh fading channel. We want that in only 1% of the cases (averaged over the offset values and the distribution of the channel) that 25% of the threshold for error floor is surpassed, resulting in

$$\int_0^\infty \Pr\left[\left|\left(\frac{DO[n]}{\mathscr{H}[n]}\right)^{(\beta)}\right| > 0.25 d_\beta\right] \cdot p_{PDF}\left(|\mathscr{H}[n]|\right) d\,|\mathscr{H}[n]| = 0.01. \tag{20}$$

TABLE V
THE ε_{min} VALUES, ε_{min} IS EXPRESSED IN % OF $\sqrt{E_s}$

Modulation	d_I	d_Q	L	ε_{min} (in %)
4 QAM ($\zeta = 1$)	0.707	0.707	4	0.525%
			8	0.743%
			16	1.051%
4 PAM	0.447	–	4	0.332%
			8	0.47%
			16	0.665%
8×4 QAM ($\zeta = 2$)	0.156	0.312	4	0.116%
			8	0.164%
			16	0.232%
16×8 QAM ($\zeta = 2$)	0.077	0.154	4	0.057%
			8	0.081%
			16	0.114%
32 PAM	0.0542	–	4	0.04%
			8	0.057%
			16	0.081%
4096 QAM ($\zeta = 1$)	0.0191	0.0191	4	0.014%
			8	0.02%
			16	0.028%

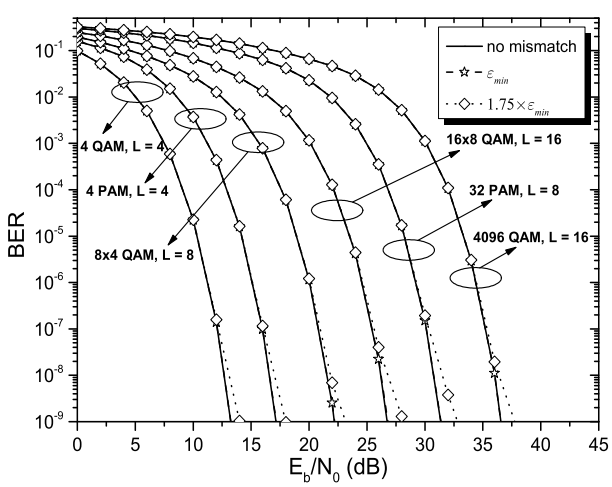

Fig. 6. BER curves for different modulation types, number of sub-ADCs and fractions of ε_{min}.

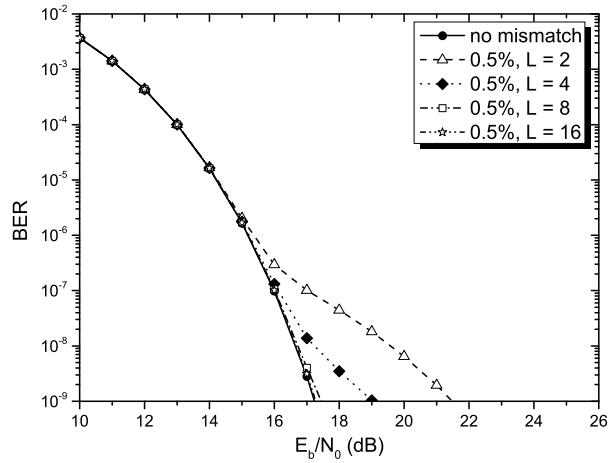

Fig. 7. BER curves for 16-QAM and different number of sub-ADCs, $\varepsilon_{min} = 0.5\%$ of $\sqrt{E_s}$.

For a Rayleigh fading channel with normalized average fading power and distribution $p_{PDF}\left(|\mathscr{H}[n]|\right) = 2\,|\mathscr{H}[n]|\, e^{-|\mathscr{H}[n]|^2}$,

TABLE VI
THE $\varepsilon_{min,Ray}$ VALUES, $\varepsilon_{min,Ray}$ IS EXPRESSED IN % OF $\sqrt{E_s}$

Modulation	d_I	d_Q	L	$\varepsilon_{min,Ray}$ (in %)
4 QAM ($\zeta = 1$)	0.707	0.707	4	0.136%
			8	0.192%
			16	0.272%
8×4 QAM ($\zeta = 2$)	0.156	0.312	4	0.03%
			8	0.042%
			16	0.06%
16 PAM	0.109	–	4	0.021%
			8	0.03%
			16	0.042%
32 PAM	0.0542	–	4	0.01%
			8	0.014%
			16	0.02%
64×32 QAM ($\zeta = 2$)	0.019	0.038	4	0.004%
			8	0.005%
			16	0.007%

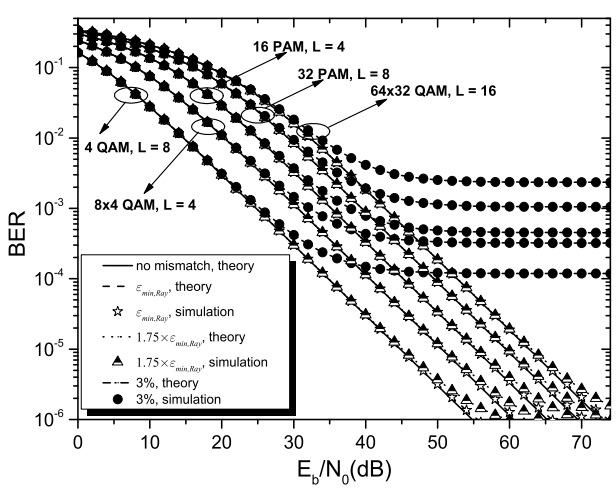

Fig. 8. BER curves in the Rayleigh fading channel for different modulation types, number of sub-ADCs and fractions of $\varepsilon_{min,Ray}$.

this results in [28, Eq. 6.287]

$$\frac{0.25 d_\beta}{\sqrt{2}\sigma_\beta[n]} = 7.018. \tag{21}$$

Similarly to the case of an AWGN channel, from (21) and assuming that the offset values are uniformly chosen in $[-\varepsilon, \varepsilon]$, we obtain the condition on the tolerable offset mismatch level ε causing an acceptable BER performance degradation in a Rayleigh fading channel: $\varepsilon \leq \varepsilon_{min,Ray}$, where $\varepsilon_{min,Ray} = \min\left(\frac{0.25\sqrt{3}d_I}{7.018\sqrt{\frac{2N}{L}}}, \frac{0.25\sqrt{3}d_Q}{7.018\sqrt{\frac{N}{L}}}\right)$ if $L > 2$, and $\varepsilon_{min,Ray} = \frac{0.25\sqrt{3}d_I}{7.018\sqrt{N}}$ if $L = 2$. Table VI shows the threshold $\varepsilon_{min,Ray}$ for different modulation types and orders, for different number L of sub-ADCs, and Fig. 8 shows the simulated and theoretical BER curves averaged over 5000 channel realization, for several cases selected from Table VI. The number of multi-path channel taps and the CP length equal 100 and 128, respectively. The channel impulse response used in simulations is modelled as a conventional exponential decaying multi-path fading channel [29]: $h[k] = \frac{1}{C}\sum_{y=0}^{99} e^{-\frac{y}{2}} A_y \delta[k-y]$, where $C = \left(\sum_{y=0}^{99} e^{-y}\right)^{1/2}$ is the normalization constant, A_y are i.i.d complex-valued Gaussian distributed random variables with zero mean and unit variance, and $\delta[.]$ denotes the discrete dirac function. Again, the simulation results well correspond to the theoretical results, which demonstrates the accuracy of the derived BER expressions. Moreover, it can be seen from the figure that, when the offset mismatch level equals the suggested threshold $\varepsilon_{min,Ray}$, there is no visible degradation with respect to the 'no mismatch' case, whereas a degradation is noticed when the mismatch level is increased to $1.75 \times \varepsilon_{min,Ray}$. Therefore, the proposed rule-of-thumb can be used in dispersive channels. Further, from Table VI and the above equations, we observe that in a dispersive channel, the tolerable offset mismatch level ε is proportional to $\sqrt{L}$, similarly as for the AWGN channel. Taking into account that in the coming years, the number of parallel sub-ADCs will further increase to achieve even higher sampling rates, the fact that the tolerable level of the offset values increases with $\sqrt{L}$ is good news, as the restrictions on the signal processing and hardware calibration algorithms to compensate for the DC offset voltages become less stringent.

VI. Conclusions

In this paper, we analysed the offset mismatch effect in TI-ADC circuits on the BER performance of an OFDM system, assuming QAM or PAM signaling and binary reflected Gray code bit mapping. For a given channel realization, exact closed-form BER expressions were analytically derived. From these BER expressions, we were able to evaluate the cause of the error floor in the BER performance at high SNRs, that is introduced by a sufficiently high offset mismatch. We showed that the maximum error floor is essentially independent of the modulation type and order, and of the channel. Moreover, we were able to analytically determine the threshold level inducing the error floor. We showed in this paper that, if we select the level of the offset mismatch so that less than 1% of the $(DO[n])^{(\beta)}$ values is larger than 25% of the threshold above which the offset mismatch causes an error floor, the BER degradation is acceptably small. This tolerable level of the offset mismatch increases with $\sqrt{L}$, indicating that the tolerable level of the offset mismatch will increase when the number of sub-ADCs increases. Based on our findings, the practical engineers, designing TI-ADCs for high-speed OFDM applications is able to extract the maximum level of the offset mismatch that can be tolerated, which can guide the circuits-and-systems design engineers that try to compensate this mismatch.

Appendix A
Derivation Of BER On Offset Mismatch-Affected Sub-carriers

1) BER on non-affected sub-carriers: In order to extend the result of [23] to offset-mismatch-affected sub-carriers, we first revisit the derivation of (9). First note that the BER of the non-affected sub-carriers, i.e., $BER_{|\mathbf{h},no\ off,n}$, can be decomposed as:

$$BER_{|\mathbf{h},no\ off,n} = \frac{1}{(m_I + m_Q)} \sum_{u,\beta} BER^{(u,\beta)}_{|\mathbf{h},no\ off,n}, \tag{22}$$

where $u \in \{1, 2, ..., m_\beta\}$ with $\beta \in \{I, Q\}$. In (22), $BER^{(u,\beta)}_{|\mathbf{h},no\ off,n}$ is the BER corresponding to bit $b_{u,\beta}$, which is the uth bit in the $\beta-$dimension, transmitted on the nth non-affected sub-carrier. The pre-factor $\frac{1}{(m_I+m_Q)}$ follows from the assumption that the bits $b_{u,\beta}$ are equally probable. In the following, we assume that the bits $b_{u,\beta}$ are mapped on the constellation points using the binary reflected Gray code (BRGC) [19]. In that case, the xth possible value of the $\beta-$dimension component, denoted as χ_x, of a constellation point (with $x \in \{0, 1, ..., 2^{m_\beta} - 1\}$ and $\beta \in \{I, Q\}$) corresponds to a bit sequence (see an example in Fig. 9)

$$\chi_x \leftrightarrow \left(\tilde{b}^{(x)}_{1,\beta}, \tilde{b}^{(x)}_{2,\beta}, ..., \tilde{b}^{(x)}_{m_\beta,\beta}\right) = (x)_2 \oplus \left(\left\lfloor \frac{x}{2} \right\rfloor\right)_2 \tag{23}$$

where $(x)_2$ denotes the natural binary code of integer x, $\lfloor x \rfloor$ denotes the largest integer smaller than x, and $\oplus$ stands for XOR operation. Taking into account that all $M_\beta = 2^{m_\beta}$ bit sequences are equally probable, $BER^{(u,\beta)}_{|\mathbf{h},no\ off,n}$ in (22) can be decomposed further as:

$$BER^{(u,\beta)}_{|\mathbf{h},no\ off,n} = \frac{1}{M_\beta} \sum_{x=0}^{2^{m_\beta}-1} BER^{(u,\beta,x)}_{|\mathbf{h},no\ off,n}. \tag{24}$$

Taking into account (3),

$$\begin{aligned} &BER^{(u,\beta,x)}_{|\mathbf{h},no\ off,n} \\ &= \Pr\left[\left(\sqrt{E_s}X[n] + \frac{W[n]}{\mathscr{H}[n]}\right)^{(\beta)} \notin \Omega^{(u,\beta,x)} | u, \beta, x\right], \end{aligned} \tag{25}$$

where $(y)^{(\beta)}$ denotes the mapping of y in the $\beta-$dimension (i.e., the real and imaginary part of y), $\mathscr{H}[n] = \sqrt{\frac{N}{N+N_{CP}}} H[n]$, and $\Omega^{(u,\beta,x)}$ is the region where the transmitted bit $b_{u,\beta}$ is decided to be equal to $\tilde{b}^{(x)}_{u,\beta}$ from (23) (see an example in Fig. 9). Note that the distance between the

boundaries of $\Omega^{(u,\beta,x)}$ and the $\beta-$dimension component χ_x of a constellation point is an odd integer multiple of d_β. As a result, $BER^{(u,\beta,x)}_{|\mathbf{h},no\ off,n}$ is of the following form:

$$BER^{(u,\beta,x)}_{|\mathbf{h},no\ off,n} = \frac{1}{2}\sum_{v=0}^{\infty}\left(\lambda_v^{(u,\beta,x)} + \rho_v^{(u,\beta,x)}\right)\cdot erfc\left((2v+1)\,d_\beta|\mathscr{H}[n]|\sqrt{\frac{E_s}{N_o}}\right), \tag{26}$$

where $\lambda_v^{(u,\beta,x)}$ and $\rho_v^{(u,\beta,x)}$ are given by:

$$\lambda_v^{(u,\beta,x)} = \begin{cases} 0 & \text{, if } \Omega^{(u,\beta,x)} \text{ has no bound at distance } (2v+1)\,d_\beta \text{ left of } \chi_x \\ (-1)^{\lfloor v\cdot 2^{u-m_\beta-1}\rfloor} & \text{, if } \Omega^{(u,\beta,x)} \text{ has a bound at distance } (2v+1)\,d_\beta \text{ left of } \chi_x \end{cases} \tag{27}$$

and

$$\rho_v^{(u,\beta,x)} = \begin{cases} 0 & \text{, if } \Omega^{(u,\beta,x)} \text{ has no bound at distance } (2v+1)\,d_\beta \text{ right of } \chi_x \\ (-1)^{\lfloor v\cdot 2^{u-m_\beta-1}\rfloor} & \text{, if } \Omega^{(u,\beta,x)} \text{ has a bound at distance } (2v+1)\,d_\beta \text{ right of } \chi_x \end{cases}, \tag{28}$$

respectively.

Substituting (24)-(26) into (22) and comparing with (9), we obtain: $R_v^{(u,\beta)} = \frac{1}{2}\sum_{x=0}^{2^{m_\beta-1}}\left(\lambda_v^{(u,\beta,x)} + \rho_v^{(u,\beta,x)}\right)$. In addition, taking into account the symmetry of the constellation symbols and the mapping rule, it is easily verified that

$$\sum_{x=0}^{2^{m_\beta-1}}\lambda_v^{(u,\beta,x)} = \sum_{x=0}^{2^{m_\beta-1}}\rho_v^{(u,\beta,x)} = R_v^{(u,\beta)}. \tag{29}$$

2) BER on affected sub-carriers: Similarly to (22)-(24), we write:

$$BER_{|\mathbf{h},\,off,n} = \frac{1}{(m_I+m_Q)}\sum_{u,\beta,x}\frac{1}{M_\beta}BER^{(u,\beta,x)}_{|\mathbf{h},off,n}, \tag{30}$$

where $BER^{(u,\beta,x)}_{|\mathbf{h},off,n}$ is the BER for the transmitted bit $b_{u,\beta}$ on an offset-mismatch-affected sub-carrier $n \in K$. Taking into account (3), $BER^{(u,\beta,x)}_{|\mathbf{h},off,n}$ can be computed as:

$$BER^{(u,\beta,x)}_{|\mathbf{h},off,n} = \Pr[(\sqrt{E_s}X[n] + \sqrt{E_s}\tfrac{DO[n]}{\mathscr{H}[n]} + \tfrac{W[n]}{\mathscr{H}[n]})^{(\beta)} \notin \Omega^{(u,\beta,x)}|u,\beta,x], \tag{31}$$

where $DO[n]$ is defined in (4). Because $\Omega^{(u,\beta,x)}$ has its boundaries at a distance that is an odd integer multiple of d_β from χ_x, (31) can be written as:

$$\begin{aligned} &BER^{(u,\beta,x)}_{|\mathbf{h},off,n} \\ &= \frac{1}{2}\sum_{v=0}^{\infty}\lambda_v^{(u,\beta,x)}\cdot \\ &erfc\left(\left((2v+1)\,d_\beta + \left(\tfrac{DO[n]}{\mathscr{H}[n]}\right)^{(\beta)}\right)|\mathscr{H}[n]|\sqrt{\tfrac{E_s}{N_0}}\right), \\ &+\frac{1}{2}\sum_{v=0}^{\infty}\rho_v^{(u,\beta,x)}\cdot \\ &erfc\left(\left((2v+1)\,d_\beta - \left(\tfrac{DO[n]}{\mathscr{H}[n]}\right)^{(\beta)}\right)|\mathscr{H}[n]|\sqrt{\tfrac{E_s}{N_0}}\right) \end{aligned} \tag{32}$$

where $\lambda_v^{(u,\beta,x)}$ and $\rho_v^{(u,\beta,x)}$ are defined as in (27) and (28), respectively.

Substituting (31)-(32) into (30) and using (29), the $BER_{|\mathbf{h},\,off,n}$ is given by:

$$\begin{aligned} &BER_{|\mathbf{h},\,off,n} = \frac{1}{2(m_I+m_Q)}\sum_{\alpha,\beta,u,v}\frac{R_v^{(u,\beta)}}{M_\beta}\cdot \\ &erfc\left(\left((2v+1)\,d_\beta + \alpha\cdot\left(\tfrac{DO[n]}{\mathscr{H}[n]}\right)^{(\beta)}\right)\left|\mathscr{H}[n]\right|\sqrt{\tfrac{E_s}{N_0}}\right), \end{aligned} \tag{33}$$

where $\alpha \in \{-1,1\}$, $\beta \in \{I,Q\}$, $u \in \{1,...,m_\beta\}$, $v \in \{0,...,(1-2^{-u})\,M_\beta - 1\}$, $M_\beta = 2^{m_\beta}$, $R_v^{(u,\beta)}$ and d_β are defined in (10) and (11), respectively, and $(DO[n])^{(\beta)}$ is defined in (5).

Appendix B
Derivation of The Maximum Error Floor

We derive the simplified expressions for the maximum error floor when the offset mismatch is very large. In that case, given that the absolute value $\left|\left(\frac{DO[n]}{\mathscr{H}[n]}\right)^{(\beta)}\right|$ is very large, one of the two expressions $(2v+1)\,d_\beta + \left(\frac{DO[n]}{\mathscr{H}[n]}\right)^{(\beta)}$ and $(2v+1)\,d_\beta - \left(\frac{DO[n]}{\mathscr{H}[n]}\right)^{(\beta)}$ is highly negative, and the other highly positive. Both expressions will contribute to the BER in (8)-(12). Taking into account that $\lim_{x\to+\infty} erfc(x) = 0$ and $\lim_{x\to-\infty} erfc(x) = 2$, it follows that the contribution from the positive expression will be negligible at high SNR, whereas the contribution from the negative expression will cause the error floor. The error floor is given by[10]:

$$\begin{aligned} BER_{r_{\max}} = &\frac{|K|_c - \eta_Q}{|I_d|_c(m_I+m_Q)}\sum_{u,v}\frac{R_v^{(u,I)}}{M_I} \\ &+\frac{|K|_c - \eta_I}{|I_d|_c(m_I+m_Q)}\sum_{u,v}\frac{R_v^{(u,Q)}}{M_Q}, \end{aligned} \tag{34}$$

where η_I and η_Q take into account that $DO[0]$ is real-valued, so that the angle of the channel coefficient $\mathscr{H}[0]$, i.e., $\varphi_{\mathscr{H}}[0]$ determines the number of terms that contribute to the BER:

$$\begin{aligned} \eta_I &= \begin{cases} 1 & \text{, if } \varphi_{\mathscr{H}}[0] = z\pi, z\in\mathbb{Z} \\ 0 & \text{, otherwise} \end{cases}, \\ \eta_Q &= \begin{cases} 1 & \text{, if } \varphi_{\mathscr{H}}[0] = \frac{\pi}{2} + z\pi, z\in\mathbb{Z} \\ 0 & \text{, otherwise} \end{cases}. \end{aligned} \tag{35}$$

[10]We assume that the sub-carrier $n = -\frac{N}{2}$ falls within the guard band, so it has no influence on the BER.

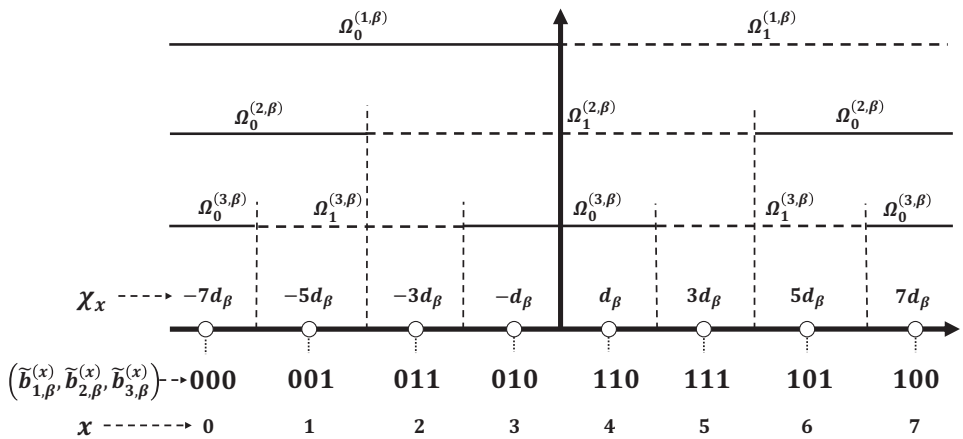

Fig. 9. BRGC mapping in the $\beta-$dimension for $m_\beta = 3$ and decision areas $\Omega^{(u,\beta)}_{\tilde{b}^{(x)}_{u,\beta}}$ with $\tilde{b}^{(x)}_{u,\beta} \in \{0,1\}$, which is a short-hand notation for $\Omega^{(u,\beta,x)}$.

TABLE VII
THE SUM $\sum_v R_v^{(u,\beta)}$

u	$R_v^{(u,\beta)}$, $v \in \{0,1,...,\left(1-2^{-u}\right)M_\beta - 1\}$	$\sum_v R_v^{(u,\beta)}$
1	$\underbrace{1,1,...,1}_{M_\beta/2}$	$M_\beta/2$
2	$\underbrace{2,2,...,2}_{M_\beta/4},\underbrace{1,1,...,1}_{M_\beta/4},\underbrace{-1,-1,...,-1}_{M_\beta/4}$	$M_\beta/2$
3	$\underbrace{4,4,...,4}_{M_\beta/8},\underbrace{3,3,...,3}_{M_\beta/8},\underbrace{-3,-3,...,-3}_{M_\beta/8},...,\underbrace{1,1,...,1}_{M_\beta/8},\underbrace{-1,-1,...,-1}_{M_\beta/8}$	$M_\beta/2$
4	$\underbrace{8,8,...,8}_{M_\beta/16},\underbrace{7,7,...,7}_{M_\beta/16},\underbrace{-7,-7,...,-7}_{M_\beta/16},...,\underbrace{1,1,...,1}_{M_\beta/16},\underbrace{-1,-1,...,-1}_{M_\beta/16}$	$M_\beta/2$
$\vdots$	$\vdots$	$\vdots$
m_β	$M_\beta/2, \left(M_\beta/2-1\right), -\left(M_\beta/2-1\right), -\left(M_\beta/2-2\right), \left(M_\beta/2-2\right),$ $...,3,-3,-2,2,1,-1$	$M_\beta/2$

Further, $|K|_c$ and $|I_d|_c$ are the cardinalities of the sets K and I_d, respectively, $R_v^{(u,\beta)}$ is defined in (10), $u \in \{1,2,...,m_\beta\}$, $v \in \{0,1,...,(1-2^{-u})M_\beta - 1\}$, and $M_\beta = 2^{m_\beta}$. The floor (34) depends on the sum of $R_v^{(u,\beta)}$ with $\beta \in \{I,Q\}$, over u and v. Table VII reveals that the sum $\sum_v R_v^{(u,\beta)}$ of $R_v^{(u,\beta)}$ over v for given u equals $\frac{M_\beta}{2}$, for all values of M_β. Hence, (34) reduces to:

$$\begin{aligned} BER_{r_{\max}} &= \frac{|K|_c - \eta_Q}{|I_d|_c(m_I+m_Q)} \cdot \frac{m_I}{2} + \frac{|K|_c - \eta_I}{|I_d|_c(m_I+m_Q)} \cdot \frac{m_Q}{2} \\ &= \frac{|K|_c}{2|I_d|_c} - \frac{m_I\eta_Q + m_Q\eta_I}{2|I_d|_c(m_I+m_Q)}. \end{aligned} \tag{36}$$

REFERENCES

[1] J. Armstrong, "OFDM for Optical Communications," *J. Lightwave Technol.,* vol. 27, no. 1, pp. 189-204, Feb. 2009.

[2] H Arslan, *Cognitive Radio, Software Defined Radio, and Adaptive Wireless Systems,* Springer, 2007.

[3] W. C. Black and D. A. Hodges, "Time Interleaved Converter Arrays," *IEEE J. Solid-State Circuits,* vol. SSC-15, no. 6, pp. 1022-1029, Dec. 1980.

[4] C. Vogel and H. Johansson, "Time-Interleaved Analog-To-Digital Converters: Status and Future Directions," *Proc. IEEE Intl. Symp. Circuits Syst.,* May 2006.

[5] S. W. Sin, S. P. U and R. P. Martins, *Generalized Low-Voltage Circuit Techniques for Very High-Speed Time-Interleaved Analog-to-Digital Converters,* Springer, 2011.

[6] A. Petraglia and S. K. Mitra, "Analysis of Mismatch Effects Among A/D Converters in a Time-Interleaved Waveform Digitizer," *IEEE Trans. Instrum. Meas.,* vol. 37, no. 5, pp. 831-835, Oct. 1991.

[7] M. Gustavsson, J. J. Wikner and N. Tan, *CMOS Data Converters for Communications,* Norwell, MA, Kluwer, 2000.

[8] N. Kurosawa, H. Kobayashi, K. Maruyama, H. Sugawara and K. Kobayashi, "Explicit Analysis of Channel Mismatch Effects in Time-Interleaved ADC Systems," *IEEE Trans. Circuits Syst.,* vol. 48, no. 3, pp. 261-271, Mar. 2001.

[9] C. Vogel, "The Impact of Combined Channel Mismatch Effects in Time-Interleaved ADCs," *IEEE Trans. Instrum. Meas.,* vol. 54, no. 1, pp. 415-427, Feb. 2005.

[10] I. N. Ku, Z. Xu, Y. C. Kuan, Y. H. Wang and M. C. F. Chang, "A 40-mW 7-bit 2.2-GS/s Time-Interleaved Subranging CMOS ADC for Low-Power Gigabit Wireless Communications," *IEEE J. Solid-State Circuits,* vol. 47, no. 8, pp. 1854-1865, Aug. 2012.

[11] S. Paquelet, G. K. D. Teyou and Y. Le. Guillou, "TI-ADCs SFDR Requirement Analysis," *IEEE Conf. New Circuits Syst.,* pp. 1-4, Jun. 2013.

[12] Y. Oh and B. Murmann, "System Embedded ADC Calibration for OFDM Receivers," *IEEE Trans. Circuits and Syst.,* vol. 53, no. 8, pp. 1693-1703, Aug. 2006.

[13] Y. Zheng, Z. Yan, J. Ma and G. He, "DC Offset Mismatch Calibration for Time-Interleaved ADCs in High-Speed OFDM Receivers," *National Conf. Comp. Engin. Tech.,* pp. 221-230, 2013.

[14] G. Keskin, J. Proesel, J. O. Plouchart and L. Pileggi, "Exploiting

Combination Redundancy for Offset Calibration in Flash ADCs," *IEEE Trans. Solid-State Circuits*, vol. 46, no. 8, pp. 1904-1918, Aug. 2011.

[15] S. Ponnuru, M. Seo, U. Madhow and M. Rodwell, "Joint Mismatch and Channel Compensation for High-Speed OFDM Receivers with Time-Interleaved ADCs," *IEEE Trans. Comm.,* vol. 58, no. 8, pp. 2391-2401, Aug. 2010.

[16] V-T-D. Huynh, N. Noels, P. Rombouts, J. Armstrong, and H. Steendam, "Effect of Time-Interleaved Analog-to-Digital Converter Mismatches on OFDM Performance," *IEEE Inter. OFDM Workshop*, pp. 128-135, Aug. 2014.

[17] J. Elbornsson, F. Gustafsson, and J-E. Eklund, "Analysis of Mismatch Effects in a Randomly Interleaved A/D Converter System" *IEEE Trans. on Circuit and Syst.*, vol. 52, no. 3, 2005.

[18] I. Guvenc, S. Gezici, Z. Sahinoglu and U. C. Kozat, *Reliable Communications for Short-range Wireless Systems,* Cambridge University Press, USA, 2011.

[19] M. Gardner, *Knotted Doughnuts and Other Mathematical Entertainments,* W.H. Freeman & Company, 1986 .

[20] H. Johansson and P. Lowenborg, "Reconstruction of Non-Uniformly Sampled Bandlimited Signals by Means of Digital fractional Delay Filters," *IEEE Trans. Signal Process.*, vol. 50, no. 11, pp. 2757-2767, Nov. 2002.

[21] R. S. Prendergast, B. C. Levy and P. J. Hurst, "Reconstruction of Band-Limited Periodic Non-Uniformly Sampled Signals Through Multi-rate Filter Banks," *IEEE Trans. Circuit and Syst.,* vol. 51, no. 3, pp. 1612-1622, Aug. 2004.

[22] W. T. Webb and L. Hanzo, *Modern Quadrature Amplitude Modulation,*, IEEE Press, 1994.

[23] K. Cho, and D. Yoon, "On the General BER Expression of One- and Two-Dimensional Amplitude Modulations," *IEEE Trans. Comm.,* vol. 50, no. 7, pp. 1074-1080, Jul. 2002.

[24] K. Cho, D. Yoon, W. Jeong and M. Kavehrad, "BER Analysis of Arbitrary Rectangular QAM," *Asilomar Conf. Sign., Syst. and Comp.,* vol. 2, pp. 1056-1059, Nov. 2001.

[25] W. Shieh and I. Djordjevic, *Orthogonal Frequency Division Multiplexing for Optical Communications,* Academic Press, USA, 2009.

[26] Y. S. Cho, J. Kim, W. Y. Yang and C. G. Kang, *MIMO-OFDM Wireless Communications with MATLAB,* Wiley-IEEE Press, 1st edition, Nov. 2010.

[27] M. K. Simon and M. S. Alouini, *Digital Communication over Fading Channels,* John Wiley & Sons, 2000.

[28] I. S. Gradshteyn and I. M. Ryzhik, *Table of Integrals, Series, and Products,* Academic Press, 1979.

[29] X. Ma, H. Kobayashi and S. C. Schwartz, "Effect of Frequency Offset on BER of OFDM and Single Carrier Systems," *IEEE Proceedings on Personal, Indoor and Mobile Radio Comm.,* vol. 3, pp. 2239-2243, Sept. 2003.

Vo-Trung-Dung Huynh was born in Vietnam, in 1987. He received the master degree in information and mechatronics from Gwangju Institute of Science and Technology, South Korea. He is currently pursuing the Ph.D. degree at the DIGCOM Research Group, Department of Telecommunications and Information Processing, Faculty of Engineering, Ghent University, Belgium. His main research interests are in digital communications, OFDM, BER performance analysis and time-interleaved analog-to-digital converter circuits.

Nele Noels (S'04, M'11) received the diploma of electrical engineering and the Ph.D. degree in electrical engineering from Ghent University, Gent, Belgium in 2001 and 2009, respectively. She is currently part-time Professor at the Department of Telecommunications and Information Processing (TELIN), Gent University and a postdoctoral researcher supported by the Research Foundation-Flanders (FWO Vlaanderen). Her main research interests are in statistical communication theory, carrier and symbol synchronization, bandwidth-efficient modulation and coding, massive MIMO, optical OFDM, satellite and mobile communication. She is (co-)author of over 40 academic papers in international journals and conference proceedings and recipient of several scientific awards. In 2010, she received the Scientific Award Alcatel Lucent Bell for the best Belgian thesis concerning an original study of information and communication technology, concepts and/or applications.

Heidi Steendam (M'01-SM'06) received the M.Sc. degree in Electrical Engineering and the Ph.D. degree in Applied Sciences from Ghent University, Gent, Belgium in 1995 and 2000, respectively. Since September 1995, she has been with the Digital Communications (DIGCOM) Research Group, Department of Telecommunications and Information Processing (TELIN), Faculty of Engineering, Ghent University, Belgium, first in the framework of various research projects, and since October 2002 as a full time Professor in the area of Digital Communications.

Her main research interests are in statistical communication theory, carrier and symbol synchronization, bandwidth-efficient modulation and coding, spread-spectrum (multi-carrier spread-spectrum), satellite and mobile communication, cognitive radio and cooperative networks. She is the author of more than 125 scientific papers in international journals and conference proceedings.

Since 2002, she is an executive Committee Member of the IEEE Communications and Vehicular Technology Society Joint Chapter, Benelux Section, and since 2012 the vice chair. She has been active in various international conferences as Technical Program Committee chair/member and Session chair. In 2004 and 2011, she was the conference chair of the IEEE Symposium on Communications and Vehicular Technology in the Benelux. She is associate editor of *IEEE Transaction on Communications*, *EURASIP Journal on Wireless Communications and Networking* and *Hindawi Journal of Computer Networks and Communications*.